

Vision-based Online Defect Detection of Polymeric Film via Structural Quality Metrics

Nathir RAWASHDEH^{1,2} , Paniz HAZAVEH¹, Safwan ALTARAZI² 

¹ Michigan Technological University, College of Computing, USA

² German Jordanian University, School of Applied Technical Sciences, Jordan

Received: 27 June 2022

Accepted: 03 January 2023

Abstract

Nondestructive and contactless online approaches for detecting defects in polymer films are of significant interest in manufacturing. This paper develops vision-based quality metrics for detecting the defects of width consistency, film edge straightness, and specks in a polymeric film production process. The three metrics are calculated from an online low-cost grayscale camera positioned over the moving film before the final collection roller and can be implemented in real-time to monitor the film manufacturing for process and quality control. The objective metrics are calibrated to correlate with an expert ranking of test samples, and results show that they can be used to detect defects and measure the quality of polymer films with satisfactory accuracy.

Keywords

Industrial inspection, Quality control, Defect detection, Polymer film, Vision.

Introduction

The market need for polymeric films is enormous and is continually growing in a wide variety of applications in food and merchandise packaging, carrier bags, as well as sensor technology in several biological and chemical fields (Film Blowing, 2023, Johnson, 2009). Various technologies are utilized to fabricate polymeric films with melt extrusion processes being the most dominant in industrial applications (Siemann, 2005; Callister & Rethwisch, 2011; Yu et al., 2004; National Research Council, 1994). Extruders, rotating screws, heated barrels, and dies are the main components that constitute such processes. High and low density polyethylene (HDPE and LDPE) and polypropylene are the most commonly used polymers in the production of polymer films (Alcan & Allaf, 2017; Gosselin et al., 2009) films made from polymer blends are also used. In film blow molding, a polymeric tube is extruded through a die. Compressed air is then blown into the tube, causing it to inflate into

a bubble-like shape. The bubble is then pulled axially into a nozzle, creating a thin cylindrical film (Belloli et al., 2012).

Production systems necessitate increasing product performance as well as increased quality control during production (Ren et al., 2022; Wang et al., 2018). The quality of a polymer film can be determined by inspecting continuous variables such as mechanical properties (such as tensile and tear strengths), optical properties (such as haze and luminous transmittance) (ASTM, 1995; ASTM D1922-15, 2020), and crystalline structure (Ajji et al., 2006). Since these assessments can be time-consuming and destructive, they are usually performed offline on a very small sample cut from the produced film (Gosselin et al., 2009; Łukasik & Stachowiak, 2020). Alternatively, since defects can have a significant impact on the quality of polymeric products, attribute-based defect detection is used to evaluate the quality of polymers (Altarazi, 2018; Shen et al., 2022). Practically, defect detection is a proven method for reducing the negative impact of product defects (Ravimal et al., 2020). In consequence, several machine-vision online techniques for inspecting polymeric film quality control and defect detection were presented.

Pratt et al. presented a machine vision inspection system for detecting defects in transparent lenses, glass and plastic sheets (Pratt & Warner, 2000). This system detects microdefects (streaks, inclusions, air

Corresponding author: Nathir Rawashdeh – Michigan Technological University, College of Computing 1400 Townsend Drive, Houghton, MI 49931, USA, phone: +1 906 487 16 11, e-mail: narawash@mtu.edu

© 2023 The Author(s). This is an open access article under the CC BY license (<http://creativecommons.org/licenses/by/4.0/>)

bubbles, grooves, cracks, etc.), and uses multiple-line scan charge-coupled device (CCD) cameras and LED light sources. For multi-layer polymer films which normally experience interfacial instabilities during their production, [Michaeli et al. \(2009\)](#) presented a structured backlight illumination approach with an image processing algorithm to detect these special types of defects. The system mainly consisted of a light source, a CCD line scan camera, and a 1D filter; was tested online and achieved 90% defects' detectability.

[Dominey and Goeckel \(2003\)](#) described a real-time-imaging film-analyzer system utilizing a camera and a high-frequency fluorescent light source. Images with defects were recorded and processed using image processing software, henceforth; defects were classified based on their size and intensity. [Johnson \(2009\)](#) developed a roll-feed imaging system to detect defects in polymer electrolyte membranes used for fuel cells. Detected defects include holes, thinning, bubbles, and gels. Additionally, the system classifies detected defects via neural networks and suggests adjustments to the manufacturing process parameters. To detect small-localized defects, [Gosselin et al. \(2009\)](#) proposed a visible-near-infrared (VIS-NIR) hyperspectral-imaging sensor for online monitoring of the LDPE/polystyrene film blend produced by extrusion blowing. By implementing multiresolution multivariate image analysis, the VIS-NIR sensor was able to clarify two factors affecting the film's mechanical properties: film ingredients composition and the stretching effect caused by pull rollers.

[Miliūnas et al. \(2017\)](#) expanded the nondestructive defects' identification of single and multilayered polymeric films, using the method of projection moiré. [Tolba and Raafat \(2015\)](#) adopted single scale and multiscale structural similarity index, as image visual quality measures, to allocate and inspect defects of flat surfaces including polymer films. The approach proposed a novel algorithm that measures the similarity of images of successive windows of a scanned film. The experimental results of the approach resulted in outstanding defect detection with an accuracy higher than 99%. [Van Drongelen et al. \(2014\)](#) integrated in situ X-ray with the extrusion process to study the structure development of LDPE. Accordingly, the development of film crystallinity and crystal structure in the bubble was determined.

Arguably, nondestructive online approaches for detecting defects in polymer films are of significant interest ([Luo et al., 2014](#); [Dong et al., 2015](#)). By avoiding the subjectivity and delay of a human-based inspection procedure or offline examination, it lowers inspection costs and improves film quality ([Johnson, 2009](#); [Tolba & Raafat, 2015](#)). On the other side, whether

compared to spectral, infrared, or X-ray imaging, an optical camera solution with real-time image processing has become a practical low-cost option.

As a result, the presented vision-based defect detection quality control approach aims to advance the nondestructive online detection of defects in polymer films, by employing an industrial inspection grade camera with integrated real-time simple and fast grayscale image processing steps ([Rawashdeh et al., 2018](#)). Extrusion-blown HDPE films are used to demonstrate the proposed approach. The presented image processing steps can be expanded for online control of film production parameters. For example, detecting the change in extruder temperature, detecting specks on the manufactured film, sensing the change in the process roller speeds, and detecting the inconsistencies in film width. In general, online quality control could instantly identify defects; hence reduce materials and energy waste.

Extrusion-blow molding

The extrusion-blow molding process for polymer film is illustrated in (Fig. 1). The process begins with the preparation of a mixture of the resin and the necessary additives such as copolymers, fillers, lubricants, etc., which are required to control the properties of the film. The mixture is fed into the extruder barrel where it is melted, mixed and conveyed under continuous pressure to a thin, round die slot. The extrudate exits into the atmosphere as a thin-walled, continuous blown tube. Next, and through nip pull rollers, the tube is rapidly drawn up. At the same time, the air ring blows cool air upward, which solidifies the tube and expands it laterally into a sausage-shaped

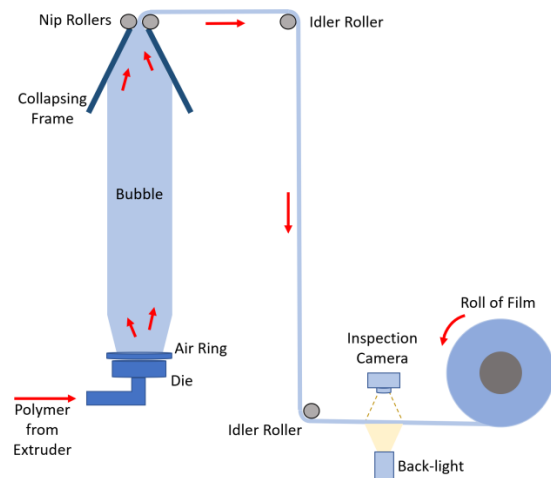


Fig. 1. Extrusion blow molding with inspection camera

bubble. The air pressure and the axial tension of the rollers cause the film extrudate to expand axially. Normally, a cage is used to control the diameter of the bubble. As the bubble enters the nip rollers it is contracted into a flat tube and then continues to cool as it moves out of the contraction tower and is rolled onto a take-up roll. More details about the extrusion blow molding process can be found in literature and online (Film Blowing, 2023; Belloli et al., 2012; Altarazi et al., 2019).

The inspection camera, described in more detail in the *Experiments* section, is installed towards the end of the process, before the film collection roller. A backlight is used to illuminate the film moving underneath the camera. The quality of the film is directly impacted by components of the mixture, their pellet sizes and percentages, preprocessing temperature, and many other material-based factors (Khan et al., 2014). The most common defects of polymer films observed in industry are listed in (Table 1) with their causes. This paper describes image processing algorithms to quantify the first three defects from a grayscale image frame of the film, i.e. Width Consistency, Edge Straightness, and Specks.

Table 1

Common defects in extruded blown polymer film and possible causes (Westlake Chemical, 2023; Alcan et al., 2017)

Film Defect	Potential Causes
Uneven film width	Faulty roller, too high or variable drawn up stress, bubble pumping or breathing, air leakage from the bubble.
Irregular film edge	Uneven roller cross-sections, variable drawn up stress.
Unwanted specks	Dirty die, non-homogenic resin.
Low gloss; High haze	Poor resin quality, improper melting temperature, improper mixing in extruder, improper cooling.
Port lines	Dirty die, low temperature for melting, die too cold or too hot.
Scratches	Dirty die or cooling cage.

To control the produced film, several parameters based on geometric characteristics of the film can be tuned. These parameters can be adjusted based on calculated metrics of defect severity or conversely, film quality. Operational parameters can also significantly affect the properties. Frequently, the following dimensionless parameters are considered (Wellstead et al., 1998): (1) the draw ratio, defines as the ratio of the

nip roller pulling speed to initial film velocity; (2) the blow up ratio, which is the ratio of the diameter of the bubble to the diameter of the circular die; (3) the frost line height defined as the height above the circular die where the molten polymer solidifies; and (4) the thickness ratio defined as the ratio of die slit to bubble thickness. The pulling speed and cooling rate of the bubble affect the thermomechanical transformations of the polymer in the bubble which, in consequence, affects its physical properties (Belloli et al., 2012; Wellstead et al., 1998). Additionally, the chemical properties can be manipulated through regulating the thermal exchange in the bubble, which also affects the width and thickness of the bubble in association with the rollers and cage constraints.

Experiments

This section summarizes the experimental details of the adopted extrusion blow film (HDPE film) and the image film-monitoring camera and lighting system. In the current extrusion blow molding study, four main material types commonly used in HDPE film production were considered. They are virgin HDPE resin, recycled HDPE, powder coated calcium carbonate (CaCO_3) filler with two different particle sizes (6 and 12 microns) and a copolymer. These solid ingredients were properly dosed and dry mixed using a mechanical mixer to produce homogeneous blends. The mixture was then extruded in a single-screw extruder. Finally, the film blowing device coupled with the extruder was used to produce the tubular film. Detailed information about the applied process has been published previously (Altarazi et al., 2019). The statistical method of mixture design was used to design the experiments for the production of the HDPE film (Altarazi & Allaf, 2017). The parameters of the blend ingredients and processing variables were included. The ranges of values for the parameters were chosen to cover a wide range of variations in the properties of the HDPE film produced. The composite constituents were recognized as the percentage of virgin HDPE, recycled HDPE, CaCO_3 , and the copolymer. The processing variables identified were the CaCO_3 mean particle size, the temperatures of the extruder heaters, extruder mixing speed, and bubble drawn up speed. The complete mixture design resulted in 86 experimental combination designs. Approximately 20-30 m of film was produced for each combination wherein image samples were implemented.

The visual inspection system consists of a five megapixel grayscale camera and a diffused white light source placed behind the moving HDPE film. The

camera and back-light are mounted towards the end of the production process before the film collection roller, as shown in (Fig. 1). This creates a back-light film view with visible edges and density as shown in (Fig. 2a). The camera is located 50 cm above the film, and the light source about 30 cm below it. This corresponds to a special resolution in the images, of around 11 pixels/mm. In order to inspect the moving HDPE film, the rate of pictures does not have to be high, since the process parameters do not change abruptly. An image frame capture and its processing for metric calculation can be performed at one-minute intervals.

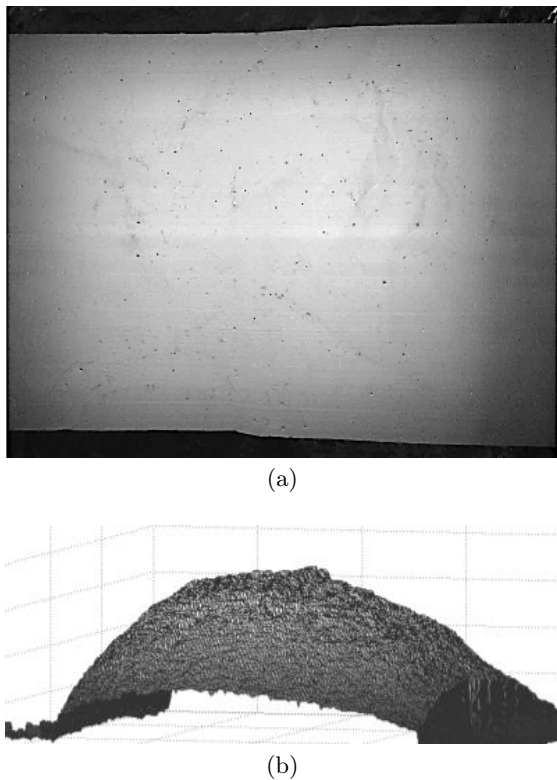


Fig. 2. Preprocessing of film image frame: (a) ROI; (b) subtracted non-uniform backlight intensity

Defect detection: quality metrics approach

To quantify overall, multi-dimensional quality of blown film production, it is necessary to numerically measure the severity of various defects, including these in (Table 1), and then develop an algorithm to combine these multiple scores, i. e. dimensions. Such an approach would be computationally and physically expensive, and may not be required by a production process that simply monitors single-dimensional qual-

ity combination algorithm. This work aims to define simple image processing-based metrics that can be used for single variate quality monitoring, primarily as an accept-reject type metric.

The underlying processing steps of the algorithms are introduced for three quality metrics that are associated with the defects of Width Consistency (WC), Edge Straightness (ES), and Specks. Initially, the image frame is prepared and enhanced. The captured image frame is processed into a grayscale region of interest (ROI) as shown in (Fig. 2a). In this image, the top and bottom edges of the film have enhanced contrast to enhance detection of film edge points. The points are used to calculate the first two metrics. In addition, the non-uniform backlight illumination, as shown in (Fig. 2b) is subtracted.

Part 1: Width Consistency metric

An important defect that degrades blown polymer film quality is uneven film width. As the blown film moves through the process several mechanical variations can cause this defect, including variable tension on the film, faulty rollers that are not perfectly cylindrical, or irregular bubble air pressure. To calculate the quality degradation due to this defect, we develop the Width Consistency metric. This metric has a dynamic range from 0 to 100, where 100 indicates zero width variation.

The percentage of the Width Consistency is calculated using the absolute difference between slopes of two lines which are fit to upper and lower edges, as shown in (1).

$$WC = 100 \times (1 - |US - LS|) \quad (1)$$

where US and LS are the slopes of fitted lines to the upper and lower edges, respectively. Note that if the absolute difference between the two slopes is greater than 1, the width consistency metric will be negative; however, this case would mean that the edges have 45 degrees of divergence, which is far below the acceptable, and a physically improbable, outcome. To illustrate the image processing steps, the upper and lower edge lines fitting are shown in (Fig. 3), and are based on about 1500 edge pixels each. These are based on the Sample 1 image shown in (Fig. 1a). There it is evident that the upper film edge has a slight positive slope US, and the lower edge has a more prominent negative slope LS. If the two slopes were similar, the absolute difference would be small, and hence the WC metric in (1) would result in a value close to 100.

The upper and lower slopes US and LS are calculated using image processing on the captured grayscale image frame, such as the one in (Fig. 2a).

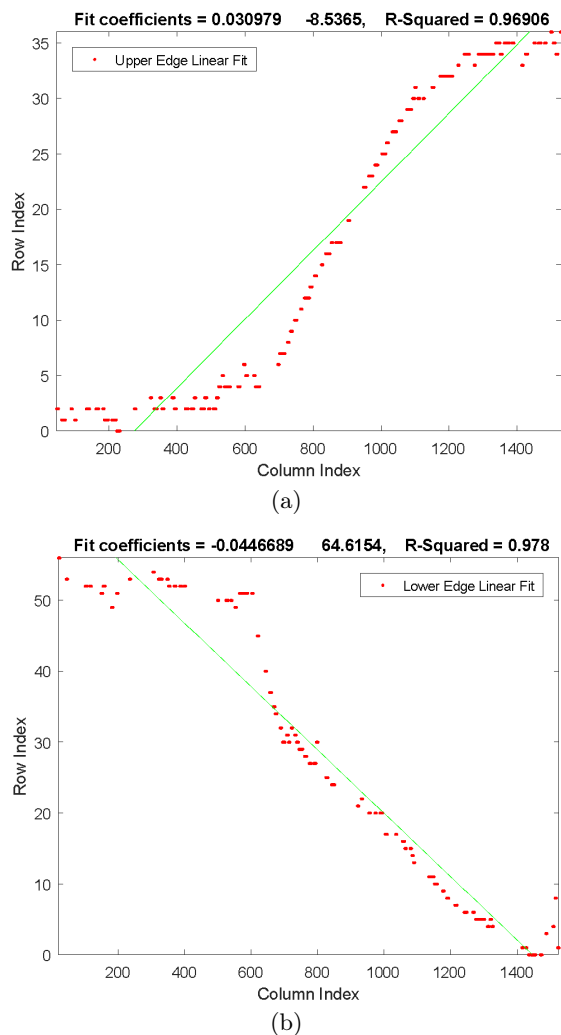


Fig. 3. Linear fit to film edge points: (a) upper edge; (b) lower edge

To find the US, horizontal edge detection is performed in the upper half of the frame. This operation yields a set of edge point x and y coordinates, or image column and row indices. Next, a line is fit to this set of points, yielding the slope value, US. The LS is found similarly, by fitting a line to the horizontal edge pixels in the lower half of the frame image.

Part 2: Edge Straightness metric

While the film may have good Width Consistency, it could suffer from non-straight, i.e., irregular edges. This can be caused by uneven roller cross-sections inducing process speed and tension variability, or uneven film thickness caused by non-homogeneous mixing of extruded ingredients. Based on the same linear fits to upper and lower film edge pixels shown in (Fig. 3), we develop a quality metric to measure

quality of Edge Straightness utilizing the fitting error. When the film has perfectly straight edges, the ES metric returns a value of 100, as (2) shows:

$$ES = 100 \times RSU \times RSL \quad (2)$$

where RSU and RSL are the R -squared goodness of line-fit measured for the upper and lower sample film edges, respectively. This value equals unity if the edge is perfectly straight and the line fit error is zero. If there is an error, the R -squared goodness value will be positive and less than unity.

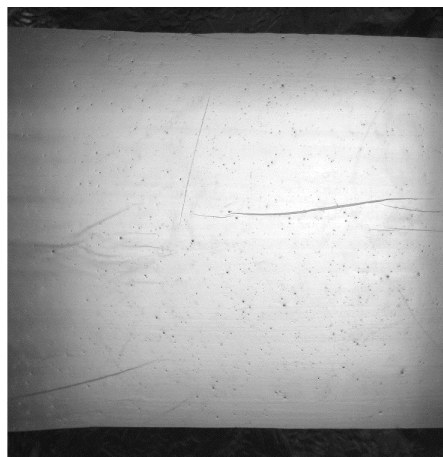
Part 3: Specks metric

Specks are grains of hard material that appear in the blown film. They can result from a nonhomogeneous resin mixture entering the extrusion process, or a dirty ring die. Quantifying the number of specks on a sample image is more processing intensive than the WC and ES metrics, because blob detection is required on the two-dimensional image region. The following is an explanation of the image processing steps required to count the number of quality degrading specks visible on the film.

Starting with the sample image, such as shown in (Fig. 4a), the first step is to choose a new rectangular ROI inside the upper and lower edges to enable blob detection. This region of interest is shown in (Fig. 4a) after: subtraction of background lighting as in (Fig. 2b); image noise removal through morphological opening; noise image smoothing through blurring; binarization to a black and white image in (Fig. 4b). The Specks' visibility is now enhanced and shown as white pixels on a black background. The subfigure shows a relatively long area of detected folding of the film, which must be subtracted. Through manual tuning, it is possible to isolate the Specks from other objects in the binary image by performing blob detection and counting the number of blobs, i. e. Specks that have a boundary length between 10 and 40 pixels. This tuning depends on the camera resolution and distance from the inspected film. (Fig. 4c) shows the isolated Specks in the sample image from (Fig. 4a). The Specks Metric (SM) is calculated using (3):

$$SM = \text{round} \left[100 \times \left(\frac{K}{K + \text{No. of Specks}} \right) \right] \quad (3)$$

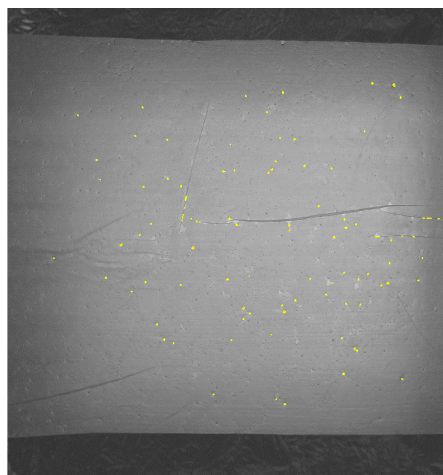
where Specks are blobs with boundary lengths between 40 and 10 pixels, and the constant $K = 200$. The value of K is chosen such that $SM = 50$ when 200 Specks are detected.



(a)



(b)



(c)

Fig. 4. Speck detection in a sample image frame: (a) original ROI before lighting correction; (b) binary image highlighting objects after dilation noise removal; (c) detected Speck boundaries of desired size

Metric correlation

The 86 experiments described in the *Experiments* section were carried out, and ten film sample images with defects were used for metric development and manual inspection. The large number of production parameter combinations is necessary to cover all possible defect scenarios. The samples, shown in (Fig. 5), are labeled as S1, through S10, and show varying degrees of defects, i.e. the three defects of interest, WC, ES, and SM. For example, S4 has a severe width inconsistency, S5 shows a large amount of specks, and S1 has poor edge straightness.

In order to develop the quantitative (objective) metrics in tune with the subjective (qualitative) observed quality, the first step is to rank sample quality subjectively by experts for each defect type. This is achieved by taking one sample, then focusing on the first defect type while comparing this sample to the other samples sequentially. This creates a subjective ranking of defect severity mimicking a customer's opinion regarding each of the three developed quality metrics.

The three proposed quantitative metrics should rank the samples under study the same way an expert observer or customer would, i. e. the apparent defect severity. This calibration is discussed in detail later in this section. In this work, four experts collectively agreed on ranking the same physical samples three times, once for each defect under study. It is somewhat challenging to ignore the multi-dimensional aspect of film quality. (Table 2) shows this subjective expert ranking of ten samples for each defect. The reader may verify the ranking by visually comparing the samples. Compared to the other samples for example, S7 has the best width consistency, but the worst edge straightness, as well as an unacceptable large amount of specks.

The asterisks in (Table 2) label the threshold after which the defect is too severe to be acceptable in the end product film. These three thresholds can be seen again in (Table 3), but here the objective calculated metric scores are shown for each of the three defects. For example, a WC or ES score below 98 means the sample is of poor quality and must be rejected, or the control process has to adapt to reduce the defect. Similarly, a Specks score less than 68 means the sample is of poor quality in regards to the amount of specks present.

The asterisks in (Table 2) label the threshold after which the defect is too severe to be acceptable in the end product film. These three thresholds can be seen again in Table 3, but here the objective calculated

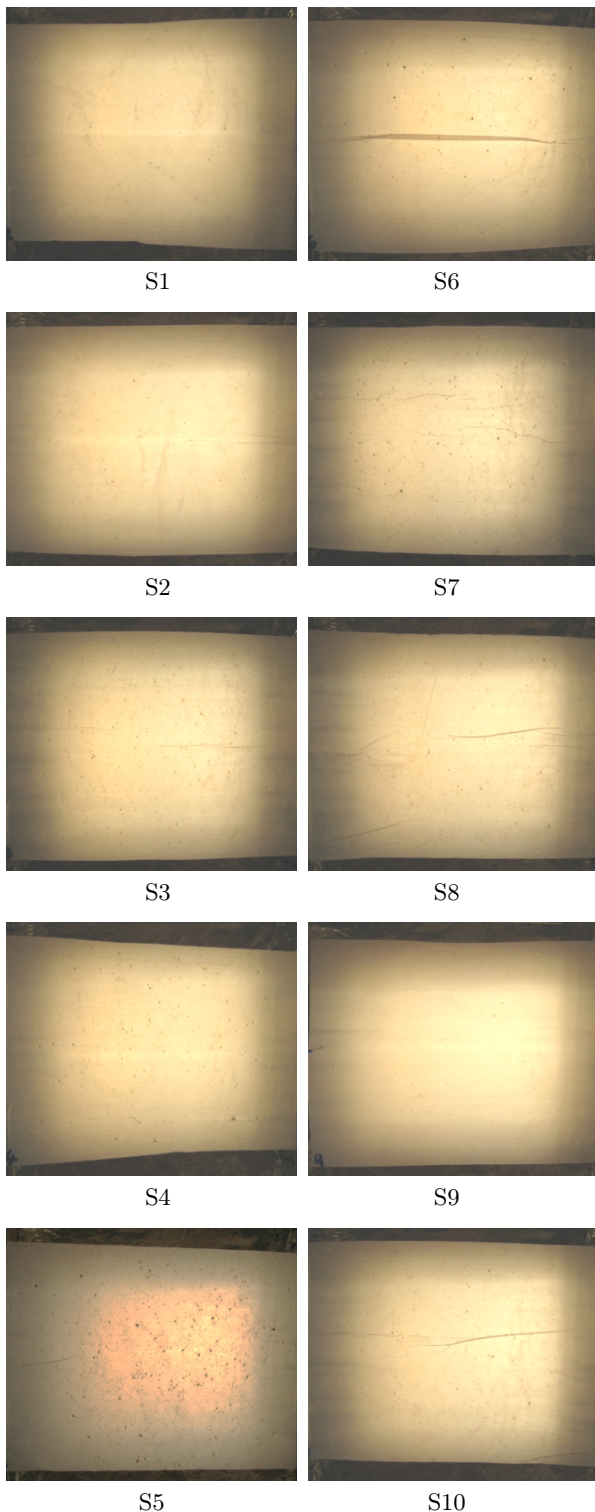


Fig. 5. Images of 10 test samples analyzed for defects

metric scores are shown for each of the three defects. For example, a WC or ES score below 98 means the sample is of poor quality and must be rejected, or the control process has to adapt to reduce the defect. Sim-

Table 2

Subjective (expert) ranking of the 10 test samples by severity of defect; sample numbers shown. An acceptability threshold is marked with an asterisk

Subjective Quality	WC	ES	SM
Highest	7	10	9
.	2	5	2
.	10	4*	1
.	9	1	10
.	8	8	8*
.	3*	6	6
.	5	3	4
.	6	2	3
.	1	9	7
Lowest	4	7	5

Table 3

Objective quality metrics for 10 test samples per proposed algorithms; quality scores shown. An acceptability threshold is marked with an asterisk

Sample #	WC	ES	SM
1	92	95	92
2	99	79	91
3	98*	81	60
4	89	98*	67
5	95	96	39
6	95	82	69
7	98	67	55
8	99	87	68*
9	98	70	96
10	99	97	71

ilarly, a Specks score less than 68 means the sample is of poor quality in regards to the amount of specks present. To show the correlation between the subjective expert rankings and the objective quality metric scores, the data in Table 2 and Table 3 is presented on two dimensional plots in Fig. 6. On the vertical axes, the metric scores are indicated from low to high. On the horizontal axes, the samples are ranked from high quality to low. A color bar indicates three levels of quality, good (green), medium (yellow), and poor (red).

The graphs show a nearly monotonically decreasing trend, proving that the objective score correlated to the subjective rankings. To increase the utility of the developed metrics, a color code is introduced on

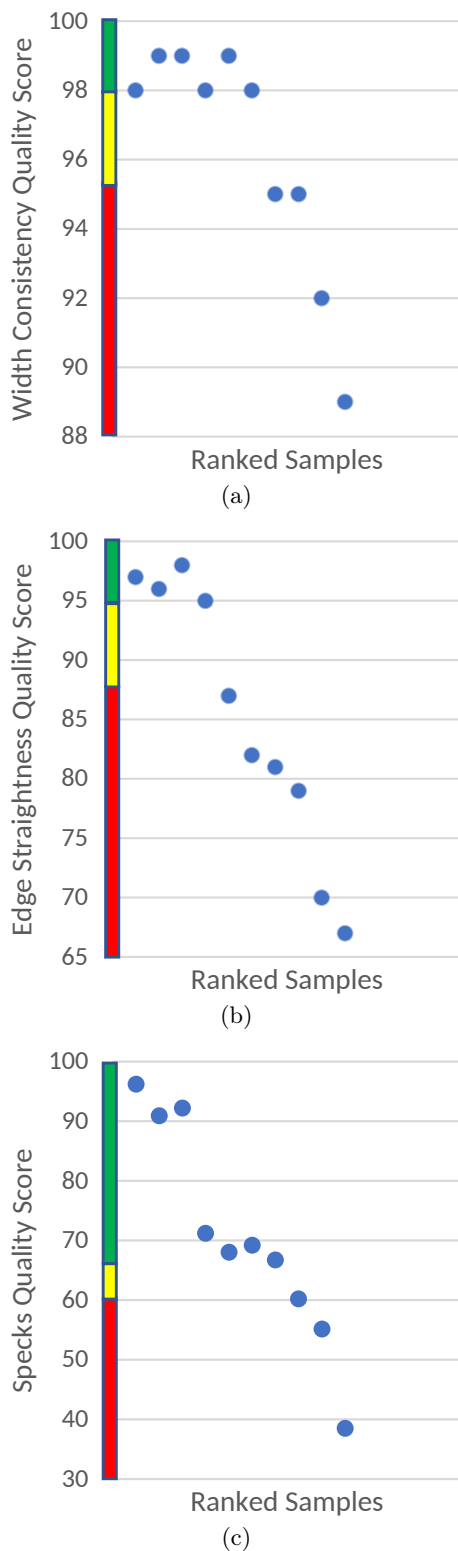


Fig. 6. Correlation between objective quality metric score (on the y-axis) and subjective expert ranking from high to low quality (on the x-axis) of polymer film samples. Point labels are Sample Numbers. The color bar indicates film quality: good (green); medium (yellow); poor (red)

the metric value, i. e. the vertical axis. Green is the range of acceptable scores which ranges from the maximum 100 down to the “worst” acceptable sample. Conversely, Red is the reject range which reaches from the score of the first rejected sample score down to zero. A medium-quality range is defined between the scores of the last accepted and the first rejected samples. The developed objective metric scores in (Table 3) are graphically represented again in (Fig. 7) as bar plots. The plot shows how the defects are apparently independent from each other. For example, S5 has a poor SM score, but relatively high scores for EC and ES. This indicates that the defect causes are also independent as discussed earlier. The bar plot colors indicate the metrics’ quality decision, i. e. accept (green) or reject (red). The only sample with all three accepted measures is sample S10.

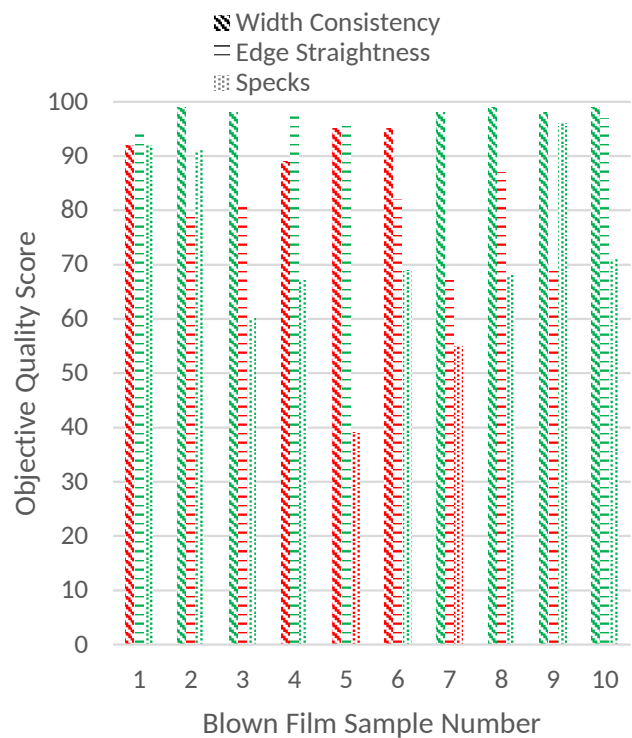


Fig. 7. Bar plot of objective metrics from (Table 3) of three defect types for samples. Color indicates the metric based quality decision: green (accept) and red (reject)

Given the independence and defects in terms of process control variables, the developed metrics in this work are one-dimensional defect detectors, rather than an overall judgment of quality, which is a function of many other defects, not examined here, and would need a more expensive system. These metrics serve as an accept-reject signal and can be logically AND-ed together to stop the process if one is a logic zero, i. e. falls below the acceptance threshold.

Metric range and variability

The three developed metrics are shown to correlate with expert rankings of test samples, which are presumably related to customer preference, as well. It is important to define the range of the metric outputs and their variability. Based on the defined ranges of quality for each metric in (Fig. 6), we can define the range and variability of each metric, given the test set. Table 4 summarized these.

Table 4

Key descriptive statistics of metric values in each quality level: good (green); medium (yellow); poor (red)

Statistic	WC	ES	SM
Green Range	(100, 98)	(100, 95)	(100, 68)
Green Mean	99	97.5	84
Green Std. Dev.	0.55	1.92	13.11
Green CV	0.56%	1.97%	15.61%
Yellow Range	(98, 95)	(95, 87)	(68, 60)
Red Range	(95, 0)	(87, 0)	(60, 0)
Red Mean	47.5	43.5	30
Red Std. Dev.	2.87	7.63	10.97
Red CV	6.04%	17.54%	36.57%

The accept (green) and reject (red) categories have a low Coefficient of Variation, i. e. the ratio of standard deviation over the mean, of around 15%. In comparison to published methods discussed in the introduction, which use labeled defects (by experts) as ground truth to assess algorithm performance, the work presented here scores the severity of three types of film defects based on expert ranking, i. e. calibra-

tion. A comparison of presented methods is provided in Table 5.

Conclusions

This paper presents three vision-based objective quality metrics for detecting polymer film defects. Namely, width consistency, edge straightness, and specks. The metrics are correlated to an expert ranking of defect severity for each defect. The results show that the objective metrics are correlated to expert ranking, and thus can be used to measure the quality of polymer films. The camera-based image processing algorithm is computationally simple and lends itself to real-time product quality monitoring and as an input to a control system that can alleviate the quality degradation of the film production process in real-time, assuming there are appropriate actuation mechanisms to change the production parameters of the running process.

Acknowledgments

Coding contribution by Laith M. Alkurdi.

References

- Ajji A. Zhang, X. and Elkoun S. (2006). Biaxial orientation in LLDPE films: Comparison of infrared spectroscopy, X-ray pole figures, and birefringence techniques, *Polym. Eng. Sci.*, Vol. 46, pp. 1182–1189.
- Alcan P., Sözüoğlu H. and Aydoğmuş S.B. (2017). Production of Market Bag and their Stability and Optimization Parameters, *Int. J. Adv. Sci. Technol.*, Vol. 103, pp. 23–34.

Table 5

A comparison of selected film and transparent material inspection

Ref.	Sensor, Light	Material, Defects	Results
(Johnson, 2009)	Roll-feed imaging system	membrane holes, thinning, bubbles, gels	Classify defects & control
(Gosselin et al., 2009)	Visible Near IR	Polystyrene film	composition and stretching
(Pratt & Warner, 2000)	Optical Camera, LED light	Lenses, glass, plastic sheets	mm2 sized defects
(Michaeli et al., 2009)	Camera & structured light	Spatial defects, polymer films	90% detection rate
(Miliūnas et al., 2017)	Optical, projection moiré	polymeric film	Single and multi-layered
(Tolba & Raafat, 2015)	Optical Camera	polymer films	99% detection rate
(Van Drongelen et al., 2014)	situ X-ray	Polyethylene extrusion	crystal structure
Self	Optical Camera & back light	Polymer film width, edge, specks	See Table 4

- Altarazi S.A. and Allaf R.M. (2017). Designing and analyzing a mixture experiment to optimize the mixing proportions of polyvinyl chloride composites, *J. Appl. Stat.*, Vol. 44, pp. 1441–1465.
- Altarazi S. (2018). Enhancing conformance of injection blow molding by integrating machine learning modeling and Taguchi parameter design, *Advances in applications and statistics*, Vol. 53, pp. 519–535.
- Altarazi S., Allaf R. and Alhindawi F. (2019). Machine Learning Models for Predicting and Classifying the Tensile Strength of Polymeric Films Fabricated via Different Production Processes, *Materials (Basel)*, Vol. 12, pp. 1475–1488.
- ASTM (1995) Subcommittee D20-10 on Mechanical Properties, Standard test method for tensile properties of thin plastic sheeting.
- ASTM (2020) D1922-15, Standard Test Method for Propagation Tear Resistance of Plastic Film and Thin Sheeting by Pendulum Method. West Conshohocken PA, ASTM International.
- Belloli D., Savaresi S.M., Cologni A., Previdi, F. and Cazola D. (2012). *Modeling and control of an Internal Bubble Cooling system*, 8th International Symposium on Mechatronics and its Applications (ISMA).
- Callister W. and Rethwisch D. (2011). *Materials science and engineering*, John Wiley & Sons, NY.
- Costin M.H., Taylor P.A. and Wright J.D. (1982). A critical review of dynamic modeling and control of plasticating extruders, *Polym. Eng. Sci.*, Vol. 22, pp. 393–401.
- Dominey S. and Goeckel W. (2003). *Polymer Defect Detection and Classification Utilizing Camera Optics*, Real Time Computation and Small Scale Resin Sample Processing, SPE.
- Dong, S., He, B., Lin, C., Zhao, Q., & Shen, H. (2015) Calibration method for a structured light measurement system with two different focal length cameras. *Measurement*, Vol. 73, pp. 462–472.
- Film Blowing (2023). *Industrial Extrusion Machinery: Blown Film Extrusion (Film Blowing)*, http://www.industrialextrusionmachinery.com/plastic_extrusion_blown_film_extrusion.html. [Accessed: 17-Jan-2023].
- Gosselin R., Rodrigue D., Ez R. and Duchesne C. (2009). Potential of hyperspectral imaging for quality control of polymer blend films, *Ind. Eng. Chem. Res.*, Vol. 48, pp. 3033–3042.
- Johnson J.T. (2009). Defect and thickness inspection system for cast thin films using machine vision and full-field transmission densitometry, (Doctoral dissertation, Georgia Institute of Technology).
- Khan J. G., Dalu R. S. and Gadekar S. S. (2014). Defects In Extrusion Process And Their Impact On Product Quality, *International journal of mechanical engineering and robotics research*, Vol. 3, pp. 187–194.
- Luo H., Xu J., Binh N.H., Liu S., Zhang C. and Chen K. (2014). A simple calibration procedure for structured light system, *Optics and Lasers in Engineering*, Vol. 57, pp. 6–12.
- Lukasik K. and Stachowiak T. (2020). Intelligent management in the age of Industry 4.0—an example of a polymer processing company, *Management and Production Engineering Review*, Vol. 11, pp. 38–49. DOI: [10.24425/mper.2020.133727](https://doi.org/10.24425/mper.2020.133727).
- Michaeli W., Berdel K. and Osterbrink O. (2009). Real-time defect detection in transparent multilayer polymer films using structured illumination and 1d filtering, *Optical Measurement Systems for Industrial Inspection VI*, No. 7389, pp. 585–593.
- Miliūnas V., Voloshin A., Kibirskštis E., Stepanenko A., Buškuvienė N. and Ragulskis L. (2017). Detection of the surface defects in thin polymeric films using projection moiré, *Journal of measurements in engineering*, Vol. 5, pp. 106–114.
- National Research Council (1994). *Polymer science and engineering: the shifting research frontiers*. National Academies Press.
- Pratt V. and Warner J. (2000). Defect inspection in transparent materials, *Sensor Review*, Vol. 20, pp. 294–298.
- Rawashdeh N.A, Abu-Khalaf J.M., Khraisat W. and Al-Hourani S.S. (2018). A visual inspection system of glass ampoule packaging defects: effect of lighting configurations, *International Journal of Computer Integrated Manufacturing*, No. 9, Vol. 31, pp. 848–856. DOI: [10.1080/0951192X.2018.1447145](https://doi.org/10.1080/0951192X.2018.1447145)
- Ravimal D., Kim H., Koh D., Hong J.H. and Lee S.K. (2020). Image-based inspection technique of a machined metal surface for an unmanned lapping process, *International Journal of Precision Engineering and Manufacturing-Green Technology*, Vol. 7, pp. 547–557.
- Ren Z., Fang F., Yan N. and Wu Y. (2022). State of the art in defect detection based on machine vision, *International Journal of Precision Engineering and Manufacturing-Green Technology*, Vol. 9, pp. 661–691.
- Shen P., Luo Z., Wang S., Mao F., Su Z. and Zhang H. (2022). Feature Detection of GFRP Subsurface Defects Using Fast Randomized Sparse Principal Component Thermography, *International Journal of Thermophysics*, Vol. 43, pp. 1–13.

- Siemann U. (2005). Solvent cast technology-A versatile tool for thin film production, *Prog. Colloid Polym. Sci.*, Vol. 130, pp. 1–14.
- Tolba A.S. and Raafat H.M. (2015). Multiscale image quality measures for defect detection in thin films, *The International Journal of Advanced Manufacturing Technology*, Vol. 79, pp. 113–122.
- Van Drongelen M., Cavallo D., Balzano L., Portale G., Vittorias I., Bras W. and Peters G.W.M. (2014). Structure Development of Low-Density Polyethylenes During Film Blowing: A Real-Time Wide-Angle X-ray Diffraction Study, *Macromol. Mater. Eng.*, Vol. 299, pp. 1494–1512.
- Wang T., Chen Y., Qiao M. and Snoussi, H. (2018). A fast and robust convolutional neural network-based defect detection model in product quality control, *The International Journal of Advanced Manufacturing Technology*, Vol. 94, pp. 3465–3471. DOI: [10.1007/s00170-017-0882-0](https://doi.org/10.1007/s00170-017-0882-0).
- Wellstead P.E., Heath W.P. and Kjaer A.P. (1998). Identification and control of web processes: Polymer film extrusion, *Control Eng. Pract.*, Vol. 6, pp. 321–331. DOI: [10.1016/S0967-0661\(97\)00023-3](https://doi.org/10.1016/S0967-0661(97)00023-3).
- Westlake Chemical (2023). *Blown Film Troubleshooting Guide*, <https://www.westlake.com/polyethylene-applications/blown-film>. [Accessed: 17–Jan–2023].
- Yu J.C., Chen X.X., Hung T.R. and Thibault F. (2004). Optimization of extrusion blow molding processes using soft computing and Taguchi's method, *J. Intell. Manuf.*, Vol. 15, pp. 625–634. DOI: [10.1023/B:JIMS.0000037712.33636.41](https://doi.org/10.1023/B:JIMS.0000037712.33636.41).